LANGMUIR

pubs.acs.org/Langmuir Article

Computational Insights into the Role of Cholesterol in Inverted Hexagonal Phase Stabilization and Endosomal Drug Release

Mohsen Ramezanpour* and D. Peter Tieleman*

Cite This: *Langmuir* 2022, 38, 7462−7471 Read Online

ACCESS | Metrics & More | Article Recommendations | Supporting Information

ABSTRACT: Cholesterol is a major component of many lipid-based drug delivery systems, including cationic lipid nanoparticles. Despite its critical role in the drug release stage, the underlying molecular mechanism by which cholesterol assists in endosomal escape remains unclear. An efficient drug release from the endosome requires endosomal disruption. This disruption is believed to involve a lamellar-to-inverted hexagonal (L_α−H_{II}) phase transition upon fusion of the lipid nanoparticle with the endosomal membrane. We used molecular dynamics simulations to study the structural properties of H_{II} systems composed of an anionic lipid distearoyl phosphatidylserine (DSPS), an ionizable cationic lipid (KC2H), and cholesterol for several hydration levels and molar ratios. This system corresponds to the lipid mixtures in the hypothesized H_{II} structure formed upon fusion and is of interest for the rational design of ionizable cationic lipids, including KC2, for an optimal drug release. Simulations suggest a geometry- and symmetry-driven lipid sorting and cholesterol−DSPS co-location around the water cores. Cholesterol preferentially co-locates with negatively charged saturated DSPS lipids at interstitial angles. The observed cholesterol−DSPS co-location results in an overall increase in the DSPS acyl chains' order parameters, which we propose to assist in stabilizing the H_{II} phase by stretching the DSPS acyl chains for filling the voids formed by three adjacent lipid tubules. Furthermore, a systematic increase in the cholesterol concentration increased the lattice plane spacing and the water core radius but decreased the undulations along the lipid tubule axis. We propose that cholesterol and the degree of saturation/polyunsaturation of the lipid acyl chains, and not the lipid charge, are the main contributors in facilitating the L_α−H_{II} phase transition and stabilizing/destabilizing the formed H_{II} phase, whereas the positive charge of the ionizable cationic lipid promotes the LNP−endosomal membrane adhesion and assists in initiating the fusion process at the local contact area. We also propose that the effect of cholesterol on the H_{II} structure and curvature is the main underlying reason for the well-documented H_{II} stabilization and destabilization at low and high molar concentrations of cholesterol, respectively.

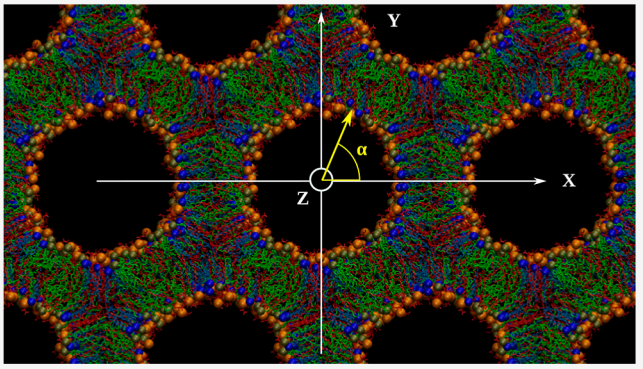

INTRODUCTION

Lipid nanoparticles (LNPs) containing ionizable cationic lipids (ICLs) are among the leading systems for small interfering RNA (siRNA) delivery in liver diseases, including cancer.[1] The first siRNA-based formulation (ONPATTRO) of this type—developed by Alnylam Pharmaceuticals, Inc.—has been recently approved by the Food and Drug Administration (FDA).[2] More recently, LNPs of this class were used in the development of messenger RNA (mRNA)-based COVID-19 vaccines by Moderna, Inc[3,4] and Pfizer/BioNTech[5,6] while many further applications are in development.

The gene release efficacy of LNPs containing ICLs (referred to as LNP from now on), however, has been reported to be, generally, quite low.[5,7−9] Only a small fraction of the delivered therapeutics to the target cells are successfully released into the cytoplasm, and the rest are degraded inside endosomes.[10−12] This is of a great importance, in particular, for mRNA formulations, mainly because the large size of mRNA molecules results in a relatively small number of mRNA molecules to be encapsulated inside the LNPs.

Assuming the LNP has successfully reached the target tissue, the polyethylene glycol (PEG)−lipid conjugates are removed from the LNPs' surface, triggering its subsequent uptake by the target cell and eventually be trapped inside the endosome where its contents need to be released into the cytoplasm for its therapeutic effect. For instance, in hepatocytes, the LNP uptake is mediated by the adsorption of apolipoprotein E (ApoE) on the LNP's surface and utilization of the ApoE-dependent

Received: February 20, 2022
Revised: May 25, 2022
Published: June 8, 2022

https://doi.org/10.1021/acs.langmuir.2c00430
Langmuir 2022, 38, 7462−7471

endocytosis mechanism, without causing the LNP lipid composition to change.[2,13,14]

The drug release level is expected to be significantly improved by using design strategies that can facilitate and accelerate the disruption process of endosomes. Before the LNP is attached to the inner (luminal) side of the endosomal membrane, the endosomal membrane is in a lamellar phase. Upon fusion of the LNP with the endosome, interactions between the components of the LNP and the endosomal membrane will result in local transient phases, for example, the H_{II} phase, which is thought to destabilize the lipid mixture at the fusion site.[15−17] According to this mechanism, one obvious strategy to enhance the drug release profile is to optimize the molecular components of the LNPs to promote and facilitate this lamellar-to-inverted hexagonal (L_α−H_{II}) phase transition and to stabilize the formed H_{II} complexes in the lipid mixture upon LNP−endosome fusion.[18] Optimizing the LNP's molecular constituents could also affect the internal structure of the LNP[19] and, therefore, enhance its drug release profile from endosomes.[20] This could be a result of different molecular packing and interactions inside the LNP or due to different interactions between the LNP and the endosomal membrane. In a study by Koltover et al.,[20] cationic LNPs with H_{II} internal structures were shown to have a higher cell transfection efficacy than complexes with lamellar internal structures; when in contact with anionic vesicles, the LNPs with an H_{II} internal structures fused rapidly to the negatively charged vesicles and released their DNA cargoes to the vesicles, whereas no fusion with the anionic vesicles was observed for the LNPs with lamellar internal structures. These observations suggest the importance of (I) the molecular composition of the LNP and (II) a role for the H_{II} phase in drug release from the endosome.

DLIN-KC2-DMA (also known as KC2) is one of the most efficacious ICLs used in LNPs for siRNA delivery.[1,2] Like other ICLs, the KC2 lipid plays multiple functions in siRNA-LNPs and the drug/gene delivery process, in general.[21] Through interactions with other LNPs comprising molecules, it promotes the molecular self-assembly and drug/gene encapsulation, in particular, for large negatively charged cargoes, such as nucleic acids. Moreover, it improves the LNP's circulation and endosomal release profiles[17] while reducing its toxicity.[21] The KC2 lipid has been rationally designed using a simple release model composed of distearoyl phosphatidylserine (DSPS) dispersions (representing the negatively charged endosomal membranes) at low pH values of ca. 4 (corresponding to the endosomal acidic environment). At this pH, KC2 is predominantly in its protonated state and thus positively charged (referred to as KC2H from now on). In equimolar mixtures, the interactions between the KC2H cationic lipids and negatively charged DSPS molecules have been proposed to result in the formation of lipid pairs consisting of one anionic and one cationic lipid with an effective truncated cone-shaped structure, which, consequently, induce a L_α−H_{II} phase transition in the DSPS membranes and destabilize this membrane by locally forming an H_{II} phase.[17]

Cholesterol is another major component of LNPs.[1,4] The properties of cholesterol/phospholipid mixtures depend strongly on the cholesterol concentration. In lipid-based drug delivery systems, cholesterol plays a critical role in the morphology and stability of LNPs and the endosomal escape of the LNP cargo.[4,22] Although the effect of cholesterol on the physical properties of LNPs and lipid membranes,[4,23−25] in general, have been studied, the role of cholesterol in the endosomal drug/gene release step is less known. One possible scenario might, however, be that cholesterol facilitates the L_α−H_{II} phase transition in the endosomal membrane upon fusion of the endosomal membrane with the LNP components. This facilitation most likely originates from cholesterol's role in stabilizing H_{II} phases in lipid mixtures as observed by a decrease of the L_α−H_{II} phase transition temperature of the mixture,[26−28] although the underlying molecular mechanism responsible for these observations is not clear. Previous reports suggest that the effect of cholesterol on the H_{II} stability and L_α−H_{II} phase transition temperature is a function of the cholesterol concentration in the lipid mixture.[27−29] A low molar concentration (between 0 and 30 mol %) of cholesterol in phosphatidylethanolamine (PE) lipid membranes[27,29] and phosphatidylcholine-PE (PC−PE) lipid mixtures[28] lowers the L_α−H_{II} phase transition temperature by increasing the relative stability of the H_{II} phase compared to the L_α phase in these systems.[26] However, cholesterol concentrations higher than 30 mol % increased the phase transition temperature.[27−32] The effect of adding cholesterol on the relative stability of L_α and H_{II} in a lipid mixture is also a function of the comprising lipids' acyl chain length and saturation,[27] so that the same mol % of cholesterol might favor stabilizing the L_α phase for one system but H_{II} for the other. Cholesterol is expected to be radially distributed around the water cores in H_{II} phases, uniformly dispersed around the phospholipids in this phase,[28,31] and modify the effective shape of the phospholipids, which might explain its role in the stabilization of the H_{II} phase at low mol % cholesterol concentrations. Nevertheless, although a low mol % of cholesterol is expected to facilitate in H_{II} formation and assist in its stabilization, there are reports on noncholesterol lipid mixtures which favor a stable H_{II} phase at some experimental conditions, for instance due to their effectively cone-shaped structures—such as PE lipids[33−37] - or due to their interactions with other biomolecules—such as nucleic acids—in the system.[19,20,38]

Computational microscopy, as a complementary technique to experiments,[39,40] could provide deeper insights and a high resolution into molecular systems of interest in drug/gene delivery,[41,42] from understanding lipoplex systems[19] to LNP-endosomal membrane fusion and endosomal escape.[43] In this study, we used molecular dynamics (MD) simulations to study the structural properties of the DSPS/KC2H/cholesterol in the H_{II} phase as a function of the composition and hydration level. These systems correspond to the lipid mixtures in the proposed H_{II} phase formed upon LNP fusion with the endosomal membrane, where KC2H is the LNP component, DSPS represents the negatively charged lipid naturally found in the endosomal membrane, and cholesterol is a major component of both LNPs and the endosomal membrane. Both DSPS/KC2H and DSPS/KC2H/cholesterol mixtures have been used for the rational design and optimization of ICLs[17,44] and as a simplified release model for evaluating the efficacy of ICLs in inducing the L_α−H_{II} phase transition and disrupting the endosomal membrane.[45] Our results provide new molecular insights into the cholesterol distribution in the H_{II} phase in this specific system and the role of cholesterol in H_{II} stabilization at a low mol % and H_{II} destabilization at a high mol % of cholesterol.

METHODS

System Construction. H_{II} phases were constructed as described in ref 46. Each lipid cylinder was comprised of either 352 (for systems containing cholesterol) or 360 (for systems with no cholesterol) lipids

https://doi.org/10.1021/acs.langmuir.2c00430
Langmuir 2022, 38, 7462−7471

with the desired molar ratio [Table 1]. In the H_{II} phase, cholesterol is expected to be mostly parallel to the phospholipid acyl chains, with its hydroxyl group near the glycerol moiety.[47−51] All lipids were initially distributed randomly on the water core surface. Assuming an N-point grid on each lipid cylinder surface, a random number generator was used to pick the desired number of points to be occupied by each lipid type to achieve the desired molar ratio. Lipid tubules were along the Z direction and filled with a water tubule of the same dimension and orientation with enough water molecules to reach the hydration level of 30 water per molecule (n_w). For systems with unequal amounts of DSPS and KC2H, water molecules were replaced by neutralizing Na^+ and Cl^- ions. This structure, that is, one lipid cylinder plus solvent, was contained in a triclinic box, and periodic boundary conditions (PBC) were applied in X, Y, and Z directions [Figure 1]. Systems with lower hydration levels were subsequently built from the systems with 30 n_w by gradually deleting a certain number of water molecules near the lipid−water interface, followed by equilibration simulations.

Table 1. Simulated H_{II} Systems and Corresponding Calculated Structural Parameters at 313 K

DSPS/KC2H/cholesterol (mol %)	water per lipid (hydration level) (n_w)[a]	d_{hex} (±SD)[b] (Å)	R_w (±SD)[b] (Å)	tubule length along Z (±SD)[b] (nm)
(50/50/0)	10	51.4 (0.3)	13.7 (0.1)	18.3 (0.2)
	15[c]	59.2 (0.5)	18.4 (0.2)	15.1 (0.3)
	20	67.2 (0.6)	23.2 (0.2)	12.7 (0.2)
	25	76.7 (0.7)	28.6 (0.3)	10.6 (0.2)
	30	84.1 (0.8)	33.0 (0.3)	9.5 (0.2)
(30/70/0)	10	45.7 (0.7)	12.3 (0.2)	23.1 (0.7)
	20	60.6 (0.7)	21.1 (0.2)	15.7 (0.3)
	30	74.9 (0.7)	29.5 (0.3)	11.9 (0.2)
(40/60/0)	10	47.8 (0.4)	12.8 (0.1)	21.1 (0.4)
	20	64.9 (0.7)	22.5 (0.2)	13.7 (0.3)
	30	80.2 (0.9)	31.5 (0.4)	10.4 (0.2)
(60/40/0)	10	52.9 (0.5)	14.1 (0.1)	17.2 (0.4)
	20	71.1 (0.6)	24.7 (0.2)	11.4 (0.2)
	30	86.5 (0.7)	34.0 (0.3)	8.9 (0.2)
(70/30/0)	10	53.6 (0.5)	14.4 (0.1)	16.8 (0.3)
	20	73.5 (0.6)	25.6 (0.2)	10.7 (0.2)
	30	92.0 (1.1)	36.2 (0.4)	7.9 (0.2)
(45/45/10)	10	51.9 (0.4)	14.1 (0.1)	16.9 (0.2)
	20	70.0 (0.7)	24.6 (0.3)	11.1 (0.2)
	30	89.5 (1.4)	35.9 (0.6)	8.0 (0.3)
(40/40/20)	10	53.8 (0.8)	15.0 (0.2)	15.0 (0.5)
	20	75.5 (0.5)	27.1 (0.2)	9.2 (0.1)
	30	94.9 (0.8)	38.6 (0.3)	6.9 (0.1)
(35/35/30)	10	57.3 (0.7)	16.3 (0.2)	12.7 (0.3)
	20	77.9 (0.6)	28.4 (0.2)	8.4 (0.1)
	30	101.3 (1.7)	41.8 (0.7)	5.9 (0.2)

[a]These values are rounded to integer n_w. The exact values are used in graphs. [b]All reported d_{hex}, R_w, tubule length along Z, and corresponding standard deviations of the mean. [c]This system was also simulated at 345 K.

Each system was energy-minimized using the steepest descent algorithm. This energy-minimized structure was used for the equilibration and production runs. Initially, a weak restraining force of 5 kJ/(mol nm^2) was applied to both the X and Y positions of each water molecule to maintain the structure of the water core, and the system was simulated in an *NPT* (constant number of particles, pressure, and temperature) ensemble for about 2−5 ns. This allowed the lipids to approach and contact the water core while allowing the size of the system in the Z direction to change slightly. Next, 5−10 ns of *NPT* simulations without position restraints were conducted to further relax the system. Finally, this structure was used for the 300 ns *NPT* simulation. The first 200 ns of each simulation was considered as the third equilibration step, during which the dimensions of the cylinder changed and equilibrated as a direct result of simulations.

Table 1 summarizes all lipid compositions, hydration levels, and temperatures. Each system was first simulated at 345 K for 300 ns, and its last frame was used to initiate further simulations at 313 K for 300 ns.

Molecular Dynamics Simulation. GROMACS software[53] version 2016.2 was used for energy minimizations and simulations with applied position restraints, whereas version 2016.3 was used for the rest. CHARMM36 force field (C36 FF) version Nov. 2016,[54] modified by adding the recently developed and validated parameters for KC2H,[55] was used to model the molecules in the system. Water molecules were described using the standard TIP3P water model[56,57] in C36 FF. All the covalent bonds involving hydrogen atoms were constrained using the LINCS[58] algorithm, and a time step of 2 fs was used in simulations. Coordinates were saved every 1 ns. The Verlet[59] scheme was used for neighbor searching. The electrostatic and van der Waals interactions were switched at 0.0 and 0.8 nm, respectively, and both were cut off at 1.2 nm. Potential-shift and force-switch functions were used as modifiers for electrostatic and van der Waals interactions, respectively. No dispersion correction was used for the van der Waals interactions. PME[60,61] was used for the treatment of long-range electrostatic interactions. Lipids and the solvent were separately coupled to a heat bath at the desired temperature. The temperature was controlled using the Nose−Hoover thermostat[62,63] with a coupling time constant of 1.0 ps. A semi-isotropic pressure coupling with a time constant of 5.0 ps was used. This allowed the pressure in the XY plane to be treated independently from the Z direction. Parrinello−Rahman[64,65] (for the 300 ns simulations) and the weak Berendsen[66] (for other steps) coupling algorithms were used to control the pressure. Using a triclinic box in the simulations required six values for each compressibility and reference pressure to be defined. To keep the box shape fixed while allowing the box sizes to scale in Z and the XY plane independently, all the diagonal components (i.e., XX, YY, and ZZ) of compressibility and reference pressure matrices were set to 4.5×10^{-5} bar^{-1} and a reference pressure of 1.0 bar, whereas other components (i.e., XY/YX, XZ/ZX, and YZ/ZY) in these matrices were set to zero. Atom coordinates and energy data were saved every 1 ns and 100 ps, respectively.

Simulation Analysis. The last 100 ns of each simulation was used for the analyses. GROMACS modules[53] and VMD[52] were used for trajectory analyses and to visualize the molecular structures, respectively.

Each reported structural parameter was calculated for each selected frame (at 1 ns intervals) and averaged over time. The standard deviations of means were also calculated from these data sets and are shown as the error bars in the graphs. For some structural parameters, such as angular distribution of lipids around the cylinder axis, averaging was done both over time and lipids.

Structural Properties of H_{II} Systems. The methods described in ref 46 were used to calculate the S_{CD} parameters and d_{hex} values for each

https://doi.org/10.1021/acs.langmuir.2c00430
Langmuir 2022, 38, 7462−7471

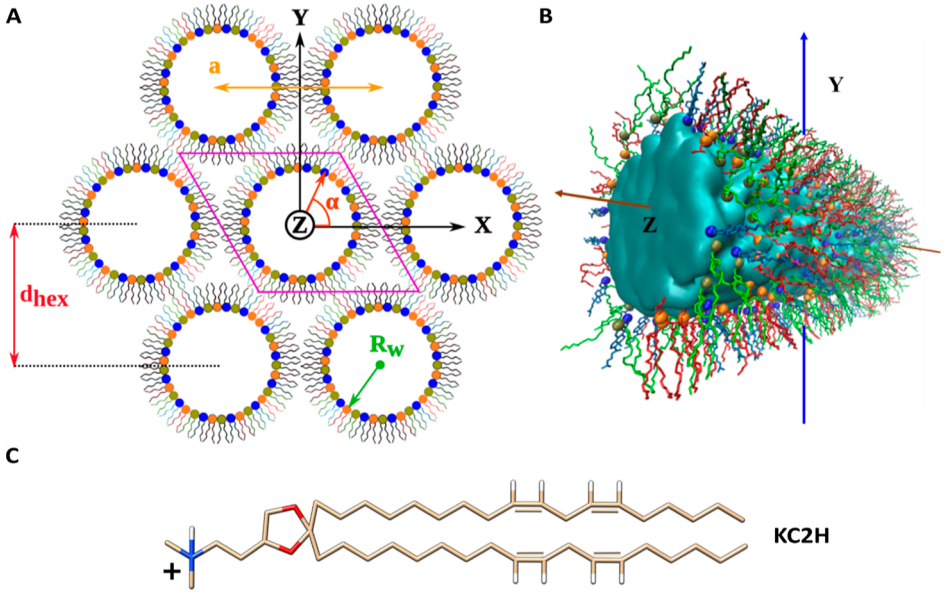

Figure 1. Lipid arrangement in the H_{II} phase (A) H_{II} structure (ternary mixture): lipid tubules filled with water and ions are arranged in a hexagonal geometry. The solvent is not shown for clarity. Each lipid cylinder is perpendicular to the *XY* plane and parallel to the *Z*-axis. Lipids are initially distributed radially and randomly around each water core. A quasi-infinite H_{II} lattice can be simulated using a single lipid tubule confined in a triclinic simulation box (shown in pink) and its periodic copies (six are shown). The radius of the water core (R_w), lattice plane distance (d_{hex}), and lattice spacing (a) parameters are illustrated. The *X* and *Y* axes point to two of the interaxial and interstitial directions, respectively. (B) Molecular view of the central lipid tubule taken from a simulated DSPS/KC2H/cholesterol (35/35/30) system with 30 n_w. The cylinder is rotated ca. 45° around the *Y*-axis for visualization purposes. The solvent is represented as the cyan surface. DSPS, KC2H, and cholesterol are shown as red, green, and light blue lines. Spheres colored in orange, tan, and dark blue represent the phosphorous atom of DSPS, nitrogen atom of KC2H, and oxygen atom of cholesterol, respectively. Hydrogens are not shown for clarity. VMD[52] was used to create the figure. (C) Chemical structure of the KC2H lipid. Oxygen, nitrogen, and hydrogen atoms are colored in red, blue, and white, respectively, whereas the carbon atoms are colored in tan. The two unsaturated bonds in each tail are shown explicitly.

simulated H_{II} system. The hydration level (n_w) was calculated by dividing the total number of water molecules trapped inside a cylinder by the total number of lipids (DSPS, KC2H, and cholesterol) covering the corresponding lipid tubule.

The water core radius (R_w) was calculated according to ref 33

$$R_w = a\sqrt{\varphi_{sol}(\sqrt{3}/2\pi)} \quad (1)$$

where a is the lattice spacing [Figure 1A] and is equal to $\left(\frac{2}{\sqrt{3}}\right)d_{hex}$, and φ_{sol} is the volume fraction of the solvent (i.e., water plus ions) inside the H_{II} cylinders. For each system, the φ_{sol} can be estimated according to ($\varphi_{sol} = V_{sol} / V_{total}$), where V_{sol} and V_{total} are the total volume taken by the solvent and the total volume of the simulation box, respectively. The V_{total} can be directly calculated from the simulations. We calculated the volume per water molecule, Na^+, and Cl^- ion at the desired temperature (e.g., 313 K) from three simulations: systems composed of (I) only 15,000 water molecules, (II) 14,900 water molecules and 100 Cl- ions, and (III) 14,900 water molecules and 100 Na^+ ions. The volume per molecule was 0.030 nm^3 for water and 0.031 nm^3 for each Na^+ and Cl^- ions.

Angular Distribution of Lipids Around the Cylinder Axis. The coordinates for the phosphorous (P) atoms of DSPS, the nitrogen (N) atoms of KC2H, and the oxygen (O) atoms of cholesterol molecules were used for this analysis. According to the cylinder length [Table 1] and its level of undulations, a cylinder was divided into several slices (rings) along the cylinder axis. Each ring was centered in the *XY* plane. The *X* and *Y* coordinates of each atom type (P, N, and O) were then used to calculate their polar angle α—the angle between the radial vector and the *X*-axis [Figure 1A] for all frames and slices and each atom type separately. Finally, a histogram from all the angles sampled by each atom type was generated. To show the overall trend in histograms more clearly, a running average over 15° was calculated.

RESULTS AND DISCUSSION

Angular Distribution of Lipids Around the Cylinder Axis. The angular distribution of lipids around the water core is shown in Figure 2. Each lipid type was initially distributed randomly. After reaching equilibrium, although each lipid type can still be found at any given angle α, the distribution of lipid types over α differs.

In systems with no cholesterol, no clear lipid sorting was observed [for example, Figure S1-A]. However, in systems containing cholesterol, the lipid sorting was clear [Figures 2 and S1 and S2], where KC2H showed the lowest deviation and cholesterol showed the largest deviation from a random distribution. This is based on the number and sharpness of extrema and the differences in frequencies between the minima and maxima in histograms [Figure S1]. This lipid sorting was, however, clearer for the systems with higher cholesterol concentrations and at higher hydration levels [Figure S1]. For instance, Figure 2 shows such lipid reorganization in DSPS/KC2H/cholesterol (35/35/30) at 313 K and 30 n_w. For this system, cholesterol has a clear tendency to be distributed along with (in other words, be co-located with) DSPS at interstitial directions (±30, ±90, and ±150), whereas KC2H is more likely to be found in the interaxial directions. For 10 n_w, a similar trend is observed [Figure S2]; that is, DSPS and cholesterol are more likely to be found in the six interstitial directions.

Effect of the Cholesterol Concentration on the Shape of DSPS/KC2H/Cholesterol Lipid Cylinders. Figure 3 shows views along the cylinder axis of lipid tubules in DSPS/KC2H/cholesterol systems with three different molar ratios simulated with 10 n_w at 313 K. Systems with 0 and 30 mol % cholesterol experienced the most and least deviations from a perfectly

https://doi.org/10.1021/acs.langmuir.2c00430
Langmuir 2022, 38, 7462−7471

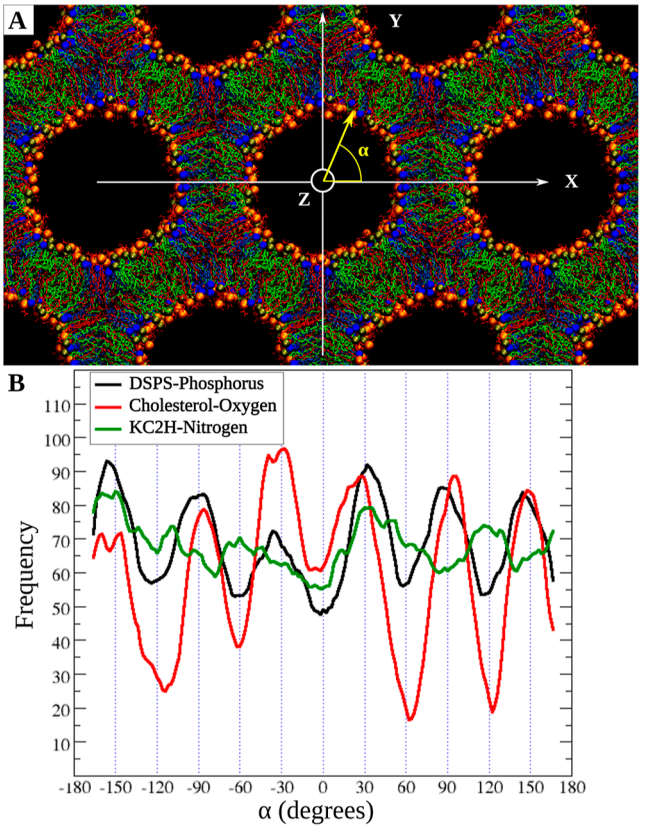

Figure 2. Lipid angular distribution around the cylinder axis. (A) Snapshot at 300 ns for the DSPS/KC2H/cholesterol (35/35/30) system with 30 n_w at 313 K. α is the polar angle with respect to the +X direction. The color code for the lipids is the same as in Figure 1B. Water and hydrogens are not shown for clarity. (B) Angular distribution of each lipid type. Black, red, and green lines are running averages over histograms of DSPS, cholesterols, and KC2H. The Y-axis shows the angular frequency for each lipid type.

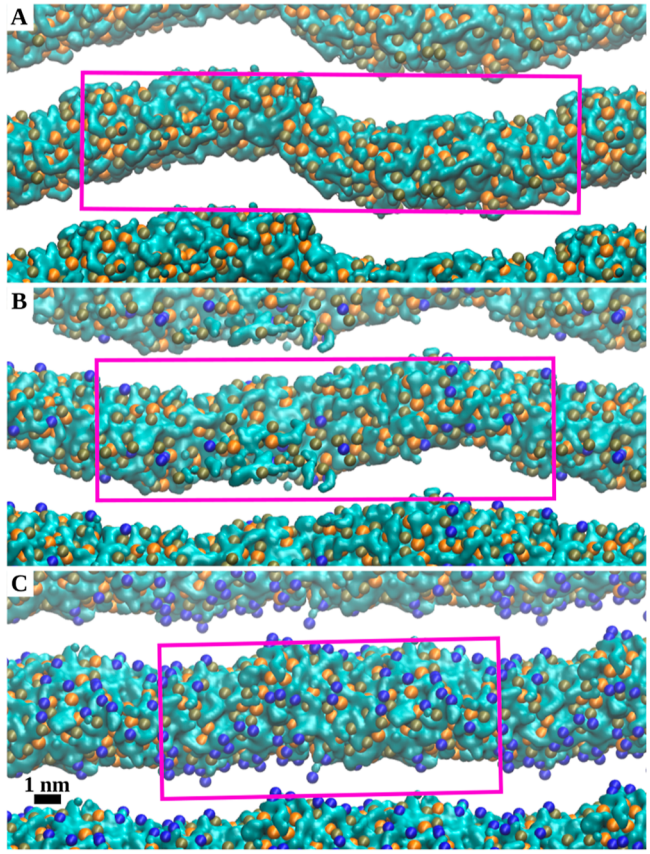

Figure 3. Effect of the cholesterol concentration on the shape of DSPS/KC2H/cholesterol lipid cylinders. The water cores in DSPS/KC2H/cholesterol systems with DSPS/KC2H/cholesterol ratios of (A) (50/50/0), (B) (45/45/10), and (C) (35/35/30) are shown. All systems correspond to simulations with 10 n_w at 313 K. The final frames of each simulated system were used to create the figures. Water is shown as a cyan surface. The orange, tan, and dark blue spheres represent the P atoms of DSPS, N atoms of KC2H, and O atoms of cholesterols, respectively. The lipid tails and cholesterols' bodies are not shown for clarity. The pink box represents the simulation box in the *ZY* plane.

straight and cylindrical tubule along the cylinder axis [Figure 3A,C]. Overall, the amplitude of these deviations decreased systematically with an increasing cholesterol concentration [Figure 3].

Lipid Sorting and Lipid−Lipid Co-location. Considering that lipids initially were distributed randomly around the water core, our key results are the observation of (I) lipid sorting and (II) co-location of cholesterol and DSPS in the DSPS/KC2H/cholesterol H_{II} systems.

Based on a previous study by Sample at al.[17] on equimolar DSPS/KC2H mixtures, the electrostatic interactions between anionic DSPS and cationic KC2H were expected to result in forming cone-shaped di-lipid ion pairs (DSPS-KC2H co-location) in this lipid mixture.

In our simulations, at least in the presence of cholesterol and under the simulated conditions, there is a clear lipid sorting where cholesterol and DSPS lipids are co-located, which does not support the DSPS−KC2H pairing scenario. However, interestingly, the structural dimensions of the systems are close to H_{II} systems composed of cone-shaped PE lipids [Figure S3]—lipids which are well-known to favor highly curved structures such as H_{II}.[33,35,67,68] The structural dimensions of the simulated (at 313 K) DSPS/KC2H/cholesterol H_{II} systems with a ratio of (50/50/0) was close to DOPE (at 323 K), whereas systems with (60/40/0) or (45/45/10) were closer to POPE (at 323 K) [Figure S3]. Clearly, increasing the cholesterol concentration in the system results in an increased R_w—equivalently decreased curvature—and increased d_{hex} values at all studied hydration levels. Moreover, in the systems with no cholesterol, an increased mol % of polyunsaturated KC2H lipids resulted in H_{II} systems with a higher curvature and smaller d_{hex} values [Figure S3].

We propose that the H_{II} geometry and symmetry, as well as the chemical structure of the constituent lipid molecules, play critical roles in the above-mentioned observations. Then, in the next two sections, we use this rationale to (I) propose an explanation for the known H_{II} stability and instability as a function of cholesterol's concentration in the system and (II) to present a new model for how cholesterol in LNPs might facilitate and accelerate gene release from endosomes by affecting the structure and stability of locally formed H_{II} phases upon fusion of the LNP with the endosomal membrane.

Geometrically, considering the structure of the H_{II} phase [Figure 1], a larger R_w results in larger void volumes formed between three adjacent cylinders,[69] which are energetically unfavorable and require lipid reorganization and sorting to optimally fill those spaces[70] [Figure 2]. The question is, which lipid distribution would be optimal and minimize the system's free energy?

https://doi.org/10.1021/acs.langmuir.2c00430
Langmuir 2022, 38, 7462−7471

The DSPS saturated tails are effectively longer than unsaturated KC2H acyl chains. The DSPS association and interactions with cholesterol increased the DSPS order parameters [Figure S4] and therefore increased the DSPS acyl chain's length. These allow DSPS acyl chains to reach the larger void volumes.[69,70] Cholesterol preferentially interacts with lipids with saturated tails over polyunsaturated lipids.[71−78] In lamellar phases, this preference is thought to be the driving force for the separation of ordered from disordered domains in saturated/unsaturated/cholesterol lipid bilayers.[74,75,79] Cholesterol is also well-known to have ordering effects on phospholipids acyl chains in lipid bilayers and to maintain its ordering effect in the H_{II} phase[30]—an ordering effect which is further a function of lipid types in the mixture.

Furthermore, the unsaturated KC2H acyl chains are less ordered and effectively shorter than DSPS acyl chains, making KC2H a good candidate for filling the thinner (compared to the ones in the interstitial directions) hydrocarbon volumes in the interaxial directions in the H_{II} phase. Furthermore, its unsaturated acyl chains allow the KC2H lipid tails to splay apart and contribute to filling the interstitial directions if needed.

If this rationalization is true, one would expect a more pronounced lipid sorting and cholesterol−DSPS co-location in H_{II} systems with a larger R_w, which is indeed supported by the simulations [Figures S1 and S2 and Figure 2]. Interestingly, there does not seem to be a strong lipid sorting in the absence of cholesterol [Figure S1]. Among the systems with no cholesterol, if any lipid sorting was energetically favorable, it was expected to be the highest for the DSPS/KC2H/cholesterol (50/50/0) system [Figure S1A] mainly because, in this case, the DSPS saturated and effectively longer tails would allow them to stretch and fill in the void's volumes, while the unsaturated and effectively shorter tails of KC2H make them the more suitable molecules to cover the interaxial distances. However, the attractive electrostatic interactions between the negatively charged DSPS and the positively charged KC2H lipids seem to enhance their co-localization and assist in H_{II} stabilization in this case, probably as proposed by Sample et al.[17] Considering that cholesterol is both a major component of LNPs and endosomal membranes, lipid mixtures containing cholesterol are a better representative of the lipid mixtures corresponding to the LNP−endosomal fusion step. Therefore, we believe that our proposed cholesterol-induced lipid sorting phenomenon and rationale for H_{II} stabilization is probably the more likely scenario to happen at that step. We hypothesize that the observed cholesterol-induced lipid sorting and cholesterol co-location with saturated lipids in the H_{II} phase could be generalized to other, for example, PE or PE/PC, lipid mixtures in this phase, especially if the lipid mixture is a saturated/polyunsaturated/cholesterol one.

Role of Cholesterol in Stabilizing the H_{II} Phase. Previous reports on the effects of cholesterol on the H_{II} phase, for example, composed of PE or PE/PC, agree that adding up to 30 mol % cholesterol (depending on the lipid type and molar ratio)[27,30,31] facilitates the formation of the H_{II} phase by lowering the L_α−H_{II} transition temperature. Increasing the cholesterol mol % higher than 30%, however, destabilizes the H_{II} phase relative to the lamellar phase.[27,29−31,69]

According to our simulations, at low molar concentrations (up to about 30 mol %), cholesterol is mostly sorted at interstitial angles and is preferentially co-located with DSPS lipids, which subsequently induces order in the DSPS acyl chains. Thus, in this way, cholesterol may assist DSPS lipids in filling the energetically unfavorable voids to effectively reduce the free energy of the system and increase the stability of the H_{II} phase. However, adding a higher mol % of cholesterol to the system increases the R_w and reduces the curvature in the H_{II} system systematically [Figure S3 and Table 1], and the voids in the H_{II} systems with a larger R_w will be larger.[69] Adding more than ∼30 mol % cholesterol reduces the curvature and increases the R_w, and consequently the void volume, up to the level where lipids cannot fill the interstitial voids anymore simply because lipid's chains must pack in an energetically unfavorable configuration and the energetic cost for such lipid packing would be too high.[69,80−83] Moreover, for such high cholesterol concentrations, there will be more cholesterol in the system than what is needed to fill the voids. The spare cholesterols might form crystalline cholesterol domains[27,29−31,69,84] or accumulate in the interaxial angles along with KC2H lipids. This is the point where the H_{II} phase is destabilized in favor of the lamellar phase (H_{II}−L_α transition). If this rationalization is true, one would expect the H_{II} system with about 40 mol % cholesterol or higher to be relatively unstable. In our simulations, we used a similar approach—which the other systems were constructed and simulated—to construct and simulate DSPS/KC2H/cholesterol H_{II} systems with 40 mol % and 50 mol % cholesterols. However, no stable H_{II} phases with circular/cylindrical water cores could form at the desired temperature and hydration level conditions for these systems.

Role of Cholesterol and KC2H in Endosomal Drug Release. Assuming LNP and endosomal membrane fusion happens and the local transient H_{II} phase forms,[15−17] the structural details of the H_{II} complex are expected to play an important role in the cargo release rates as well although its effects on release rates might be small for large molecules such as mRNA. Considering that cholesterol affects the H_{II} structure [Figure 2, Figure 3, and S2−S4], we propose that the mol % of cholesterol plays a key role in the endosomal release of drugs.

While our simulations do not address the role of KC2H (a polyunsaturated ionizable cationic lipid) in endosomal drug release directly, it clearly suggests that neither the KC2H positive charge nor the DSPS−KC2H (anionic−cationic) lipids interactions are the main contributors in forming a stable H_{II} phase. Instead, it seems that (I) the polyunsaturated acyl chains and molecular shape of KC2H, (II) the saturated acyl chains of DSPS, and most importantly, (III) the preferential interactions and effects of cholesterol on saturated and polyunsaturated lipids in the system play the main roles in this step. Upon LNP−endosome fusion, a local saturated/polyunsaturated/cholesterol mixture forms. The cholesterol−lipid interactions will result in forming local transient lipid domains where cholesterol mostly interacts with the saturated lipids (e.g., DSPS−cholesterol), and the polyunsaturated lipids (e.g., KC2H) form separate domains. These domains—due to their different effective shapes and rigidity level—induce local transient curvatures and the LNP−endosomal membrane contacts, which could initiate the L_α−H_{II} transition process.

If the positive charge of KC2H is not critical for H_{II} formation and stabilization, what other role(s) might it play in the drug release stage? Although our simulations do not provide any data related to the adhesion and fusion parts directly, we propose that the positive charge of KC2H lipids on the LNP's surface is critical in (I) promoting the LNP adhesion to the inner side of endosomes and keeping their molecular constituents in a close contact for enough time allowing their mixing to start, and (II) interacting with the negatively charged lipids in both the inner

https://doi.org/10.1021/acs.langmuir.2c00430
Langmuir 2022, 38, 7462−7471

and outer leaflets of the endosomal membrane, allowing local transient disruptions, for example, forming pores, required for the LNP−endosome membrane fusion process to be initiated.[16] The fusion process has a high energetic barrier,[85,86] and having a driving force to bring two membranes together is a key step in fusion. That is indeed what SNARE proteins in synaptic vesicles and fusion peptides in viruses do.[87−89] The lack of positively charged KC2H on the LNP's surface—which seems to be the case for LNP formulations containing KC2(H) under physiological pH levels[55,90]— will cause a delay in the LNP−endosome adhesion and consequently, a delay in fusion, endosomal membrane disruption, and drug release.

Model Limitations and Considerations. This study is based on the main assumption that when an LNP adheres to the internal side of the endosomal membrane, they fuse together, a L_α−H_{II} phase transition happens, and an H_{II} phase forms in the mixture.[15−17] However, the real scenario might be more complex, and indeed multiple transient phases might co-exist upon fusion. Unfortunately, given the current resolution of experimental techniques, it is impossible to detect and get a deeper insight into the details of this critical stage during drug release. A much more complex simulation setup could look at the fusion of a preassembled loaded LNP with a modeled endosomal membrane and explore the structure and dynamics of the mixture upon fusion and the mechanism of drug release from those complexes. However, this might be a major challenge both in time and length scales. The recent advances in computational hardware and algorithms have made it possible to use simplified systems to approximate and tackle the LNP−endosomal membrane fusion and gene release steps computationally.[43]

This study was based on a simple release model using DSPS as the anionic lipid component of the endosomal membrane, matching experiments on this system. A more realistic future release model would include lysobisphosphatidic acids[91] and other known endosomal lipid components.[92]

The simulation times, level of sampling, system size, and geometric limitations used in the simulations are also important and may affect the results. Although the current simulations clearly suggest a tendency for lipid sorting and cholesterol−DSPS co-location in the H_{II} phase, reaching a symmetric (converged) angular distribution profile requires much longer simulation times (probably microseconds) to allow lipids to diffuse both laterally along the lipid cylinder and radially around the water core. Regarding the system size, there are studies suggesting that the system size could affect the undulations in lipid bilayers.[93] Using coarse-grained models such as MARTINI[94−96] allows such longer simulation times and enough sampling, as well as simulating larger molecular systems closer in scale to the experimental systems. However, the lower chemical resolution is a significant approximation in interpreting the detailed molecular interactions and confined water.

The exact hydration level for different lipid compositions studied in the H_{II} phase is not known, which we addressed by simulating a range of plausible hydration levels, including more hydrated than likely experimentally. The maximum hydration level for only one of the systems where the experimental data are available for[45] can be estimated to be around 11.1 n_w [see the SI Methods section, Figure S7]. Moreover, the total number of molecules is fixed over the course of simulations. Therefore, any water exchange between the water cores and excess water, which is possible in experimental setups, is prohibited as a direct result of the simulation setup.[46]

CONCLUSIONS

MD simulation of DSPS/KC2H/cholesterol mixtures in the H_{II} phase was used to investigate the cholesterol's roles in H_{II} stabilization and consequently on endosomal membrane disruption and drug/gene release.

In the presence of cholesterol, there is a strong tendency for lipid sorting around the water core, where cholesterol and DSPS lipids are more likely to be co-located and point to the six interstitial directions, whereas KC2H lipids will populate the interaxial directions. Although the geometry is different, these observations are in line with well-known properties of tertiary mixtures of cholesterol, saturated and unsaturated lipids, in which cholesterol co-locates preferentially with saturated lipids.[76−78] We propose that both this sorting and cholesterol−DSPS co-location in the H_{II} phase play critical roles in H_{II} stabilization at low mol % (up to ∼30 mol %) of cholesterol. A higher mol % of cholesterol, on the other hand, decreases the curvature to such an extent that the H_{II} phase becomes energetically unfavorable compared to the lamellar phase, favoring the H_{II}−L_α phase transition (reverse L_α−H_{II} transition). Moreover, the presence of cholesterol rigidifies the lipid tubules and reduces their undulations along their axis. Finally, the structural dimensions of the DSPS/KC2H/cholesterol H_{II} systems were similar to those for H_{II} systems composed of cone-shaped PE lipids.

We proposed several models and explanations for how cholesterol sorting and co-location with saturated lipids and the presence of positively charged KC2H lipid with polyunsaturated tails could assist in the endosomal membrane disruption and drug release by promoting and stabilizing H_{II} systems which are formed after LNP−endosomal membrane fusion. Our model can be used to explain how H_{II} stability is affected as a function of the cholesterol concentration in the mixture. Finally, we hypothesize that the positive charge of KC2H is more likely to play a key role in the LNP adhesion to the endosomal membrane and in initiating their membranes fusion rather than in L_α−H_{II} phase transition or H_{II} stabilization.

ASSOCIATED CONTENT

Supporting Information

The Supporting Information is available free of charge at https://pubs.acs.org/doi/10.1021/acs.langmuir.2c00430.

Lipid sorting in DSPS/KS2H/cholesterol H_{II} systems; comparing the structural parameters between DSPS/KC2H/cholesterol systems with H_{II} systems composed of DOPE and POPE; simulation setup validation; and estimation of maximum hydration for DSPS/KC2H/cholesterol (45/45/10) at 310 K (PDF)

AUTHOR INFORMATION

Corresponding Authors

Mohsen Ramezanpour − *Centre for Molecular Simulation, Department of Biological Sciences, University of Calgary, Calgary AB T2N 1N4, Canada;* orcid.org/0000-0002-5333-0068; Email: ramezanpour.mohsen@gmail.com

D. Peter Tieleman − *Centre for Molecular Simulation, Department of Biological Sciences, University of Calgary, Calgary AB T2N 1N4, Canada;* orcid.org/0000-0001-5507-0688; Email: tieleman@ucalgary.ca

Complete contact information is available at: https://pubs.acs.org/10.1021/acs.langmuir.2c00430

https://doi.org/10.1021/acs.langmuir.2c00430
Langmuir 2022, 38, 7462−7471

Notes

The authors declare no competing financial interest.

■ ACKNOWLEDGMENTS

Work in the D.P.T.s group is supported by the Natural Sciences and Engineering Research Council (Canada). Further support came from the Canada Research Chairs program. Calculations were carried out on Compute Canada facilities, supported by the Canada Foundation for Innovation and partners.

■ ABBREVIATIONS

LNP, lipid nanoparticle; MD, molecular dynamics; H_{II}, reverse/inverted hexagonal phase; ICL, ionizable cationic lipid; KC2(H), DLin-KC2-DMA ionizable cationic lipid; KC2H, the protonated form of KC2(H); KC2, the neutral form of KC2(H); PE, phosphatidylethanolamine; POPE, palmitoyl-oleoyl phosphatidylethanolamine; DOPE, dioleoyl phosphatidylethanolamine; DSPS, distearoyl phosphatidylserine; S_{CD}, deuterium order parameter for the C−D bond; d_{hex}, lattice plane distance; a, lattice spacing; R_w, water core radius; n_w, water molecules per lipid inside the lipid cylinder (or equivalent hydration level); FF, force field; C36 FF, CHARMM36 force field; siRNA, small interfering RNA; mRNA, messenger RNA La

■ REFERENCES

(1) Cullis, P. R.; Hope, M. J. Lipid nanoparticle systems for enabling gene therapies. *Mol. Ther.* **2017**, *25*, 1467−1475.
(2) Akinc, A.; Maier, M. A.; Manoharan, M.; Fitzgerald, K.; Jayaraman, M.; Barros, S.; Ansell, S.; Du, X.; Hope, M. J.; Madden, T. D.; Mui, B. L.; Semple, S. C.; Tam, Y. K.; Ciufolini, M.; Witzigmann, D.; Kulkarni, J. A.; van der Meel, R.; Cullis, P. R. The Onpattro story and the clinical translation of nanomedicines containing nucleic acid-based drugs. *Nat. Nanotechnol.* **2019**, *14*, 1084−1087.
(3) Moderna. Moderna's work on a potential vaccine against COVID-19. https://www.modernatx.com/modernas-work-potential-vaccine-against-covid-19 (accessed on May 9, 2021).
(4) Eygeris, Y.; Patel, S.; Jozic, A.; Sahay, G. Deconvoluting lipid nanoparticle structure for messenger RNA delivery. *Nano Lett.* **2020**, *20*, 4543−4549.
(5) Kim, J.; Eygeris, Y.; Gupta, M.; Sahay, G. Self-assembled mRNA vaccines. *Adv. Drug Delivery Rev.* **2021**, *170*, 83−112.
(6) Hou, X.; Zaks, T.; Langer, R.; Dong, Y. Lipid nanoparticles for mRNA delivery. *Nat. Rev. Mater.* **2021**, *6*, 1078.
(7) Gilleron, J.; Querbes, W.; Zeigerer, A.; Borodovsky, A.; Marsico, G.; Schubert, U.; Manygoats, K.; Seifert, S.; Andree, C.; Stöter, M.; Epstein-Barash, H.; Zhang, L.; Koteliansky, V.; Fitzgerald, K.; Fava, E.; Bickle, M.; Kalaidzidis, Y.; Akinc, A.; Maier, M.; Zerial, M. Image-based analysis of lipid nanoparticle−mediated siRNA delivery, intracellular trafficking and endosomal escape. *Nat. Biotechnol.* **2013**, *31*, 638−646.
(8) Sabnis, S.; Kumarasinghe, E. S.; Salerno, T.; Mihai, C.; Ketova, T.; Senn, J. J.; Lynn, A.; Bulychev, A.; McFadyen, I.; Chan, J.; Almarsson, Ö.; Stanton, M. G.; Benenato, K. E. A novel amino lipid series for mRNA delivery: improved endosomal escape and sustained pharmacology and safety in non-human primates. *Mol. Ther.* **2018**, *26*, 1509−1519.
(9) Xu, E.; Saltzman, W. M.; Piotrowski-Daspit, A. S. Escaping the endosome: Assessing cellular trafficking mechanisms of non-viral vehicles. *J. Controlled Release* **2021**, *335*, 465−480.
(10) Sahay, G.; Querbes, W.; Alabi, C.; Eltoukhy, A.; Sarkar, S.; Zurenko, C.; Karagiannis, E.; Love, K.; Chen, D.; Zoncu, R.; Buganim, Y.; Schroeder, A.; Langer, R.; Anderson, D. G. Efficiency of siRNA delivery by lipid nanoparticles is limited by endocytic recycling. *Nat. Biotechnol.* **2013**, *31*, 653−658.
(11) Suh, J.; An, Y.; Tang, B. C.; Dempsey, C.; Huang, F.; Hanes, J. Real-time gene delivery vector tracking in the endo-lysosomal pathway of live cells. *Microsc. Res. Tech.* **2012**, *75*, 691−697.
(12) Nguyen, J.; Szoka, F. C. Nucleic acid delivery: The missing pieces of the puzzle? *Acc. Chem. Res.* **2012**, *45*, 1153−1162.
(13) Kulkarni, J. A.; Witzigmann, D.; Chen, S.; Cullis, P. R.; van der Meel, R. Lipid nanoparticle technology for clinical translation of siRNA therapeutics. *Acc. Chem. Res.* **2019**, *52*, 2435−2444.
(14) Kulkarni, J. A.; Cullis, P. R.; Van Der Meel, R. Lipid nanoparticles enabling gene therapies: from concepts to clinical utility. *Nucleic Acid Ther.* **2018**, *28*, 146−157.
(15) Hafez, I.; Maurer, N.; Cullis, P. On the mechanism whereby cationic lipids promote intracellular delivery of polynucleic acids. *Gene Ther.* **2001**, *8*, 1188−1196.
(16) Hafez, I. M.; Cullis, P. R. Roles of lipid polymorphism in intracellular delivery. *Adv. Drug Delivery Rev.* **2001**, *47*, 139−148.
(17) Semple, S. C.; Akinc, A.; Chen, J.; Sandhu, A. P.; Mui, B. L.; Cho, C. K.; Sah, D. W. Y.; Stebbing, D.; Crosley, E. J.; Yaworski, E.; Hafez, I. M.; Dorkin, J. R.; Qin, J.; Lam, K.; Rajeev, K. G.; Wong, K. F.; Jeffs, L. B.; Nechev, L.; Eisenhardt, M. L.; Jayaraman, M.; Kazem, M.; Maier, M. A.; Srinivasulu, M.; Weinstein, M. J.; Chen, Q.; Alvarez, R.; Barros, S. A.; De, S.; Klimuk, S. K.; Borland, T.; Kosovrasti, V.; Cantley, W. L.; Tam, Y. K.; Manoharan, M.; Ciufolini, M. A.; Tracy, M. A.; de Fougerolles, A.; MacLachlan, I.; Cullis, P. R.; Madden, T. D.; Hope, M. J. Rational design of cationic lipids for siRNA delivery. *Nat. Biotechnol.* **2010**, *28*, 172−176.
(18) Lu, J. J.; Langer, R.; Chen, J. A novel mechanism is involved in cationic lipid-mediated functional siRNA delivery. *Mol. Pharm.* **2009**, *6*, 763−771.
(19) Corsi, J.; Hawtin, R. W.; Ces, O.; Attard, G. S.; Khalid, S. DNA lipoplexes: formation of the inverse hexagonal phase observed by coarse-grained molecular dynamics simulation. *Langmuir* **2010**, *26*, 12119−12125.
(20) Koltover, I.; Salditt, T.; Rädler, J. O.; Safinya, C. R. An inverted hexagonal phase of cationic liposome-DNA complexes related to DNA release and delivery. *Science* **1998**, *281*, 78−81.
(21) Tam, Y.; Chen, S.; Cullis, P. Advances in lipid nanoparticles for siRNA delivery. *Pharmaceutics* **2013**, *5*, 498−507.
(22) Briuglia, M.-L.; Rotella, C.; McFarlane, A.; Lamprou, D. A. Influence of cholesterol on liposome stability and on in vitro drug release. *Drug Delivery Transl. Res.* **2015**, *5*, 231−242.
(23) Patel, S.; Ashwanikumar, N.; Robinson, E.; Xia, Y.; Mihai, C.; Griffith, J. P.; Hou, S.; Esposito, A. A.; Ketova, T.; Welsher, K. Naturally-occurring cholesterol analogues in lipid nanoparticles induce polymorphic shape and enhance intracellular delivery of mRNA. *Nat. Commun.* **2020**, *11*, 983.
(24) Pozzi, D.; Marchini, C.; Cardarelli, F.; Amenitsch, H.; Garulli, C.; Bifone, A.; Caracciolo, G. Transfection efficiency boost of cholesterol-containing lipoplexes. *Biochim. Biophys. Acta, Biomembr.* **2012**, *1818*, 2335−2343.
(25) Tenchov, B. G.; MacDonald, R. C.; Siegel, D. P. Cubic phases in phosphatidylcholine-cholesterol mixtures: cholesterol as membrane "fusogen". *Biophys. J.* **2006**, *91*, 2508−2516.
(26) Cheng, X.; Lee, R. J. The role of helper lipids in lipid nanoparticles (LNPs) designed for oligonucleotide delivery. *Adv. Drug Delivery Rev.* **2016**, *99*, 129−137.
(27) Cheetham, J. J.; Wachtel, E.; Bach, D.; Epand, R. M. Role of the stereochemistry of the hydroxyl group of cholesterol and the formation of nonbilayer structures in phosphatidylethanolamines. *Biochemistry* **1989**, *28*, 8928−8934.
(28) Tilcock, C. P. S.; Bally, M. B.; Farren, S. B.; Cullis, P. R. Influence of cholesterol on the structural preferences of dioleoylphosphatidylethanolamine-dioleoylphosphatidylcholine systems: A phosphorus-31 and deuterium nuclear magnetic resonance study. *Biochemistry* **1982**, *21*, 4596−4601.
(29) Epand, R. M.; Bottega, R. Modulation of the phase transition behavior of phosphatidylethanolamine by cholesterol and oxysterols. *Biochemistry* **1987**, *26*, 1820−1825.
(30) Paré, C.; Lafleur, M. Polymorphism of POPE/cholesterol system: A 2H nuclear magnetic resonance and infrared spectroscopic investigation. *Biophys. J.* **1998**, *74*, 899−909.

https://doi.org/10.1021/acs.langmuir.2c00430
Langmuir 2022, 38, 7462−7471

(31) Takahashi, H.; Sinoda, K.; Hatta, I. Effects of cholesterol on the lamellar and the inverted hexagonal phases of dielaidoylphosphatidylethanolamine. *Biochim. Biophys. Acta, Gen. Subj.* **1996**, *1289*, 209−216.
(32) Gallay, J.; De Kruijff, B. Correlation between molecular shape and hexagonal HII phase promoting ability of sterols. *FEBS Lett.* **1982**, *143*, 133−136.
(33) Tate, M. W.; Gruner, S. M. Temperature dependence of the structural dimensions of the inverted hexagonal (H_{II}) phase of phosphatidylethanolamine-containing membranes. *Biochemistry* **1989**, *28*, 4245−4253.
(34) Turner, D. C.; Gruner, S. M. X-ray diffraction reconstruction of the inverted hexagonal (H_{II}) phase in lipid-water systems. *Biochemistry* **1992**, *31*, 1340−1355.
(35) Harper, P. E.; Mannock, D. A.; Lewis, R. N. A. H.; McElhaney, R. N.; Gruner, S. M. X-ray diffraction structures of some phosphatidylethanolamine lamellar and inverted hexagonal phases. *Biophys. J.* **2001**, *81*, 2693−2706.
(36) Rand, R. P.; Fuller, N. L. Structural dimensions and their changes in a reentrant hexagonal-lamellar transition of phospholipids. *Biophys. J.* **1994**, *66*, 2127−2138.
(37) Rappolt, M.; Hickel, A.; Bringezu, F.; Lohner, K. Mechanism of the lamellar/inverse hexagonal phase transition examined by high resolution X-ray diffraction. *Biophys. J.* **2003**, *84*, 3111−3122.
(38) Angelov, B.; Garamus, V. M.; Drechsler, M.; Angelova, A. Structural analysis of nanoparticulate carriers for encapsulation of macromolecular drugs. *J. Mol. Liq.* **2017**, *235*, 83−89.
(39) Ingólfsson, H. I.; Arnarez, C.; Periole, X.; Marrink, S. J. Computational 'microscopy'of cellular membranes. *J. Cell Sci.* **2016**, *129*, 257−268.
(40) Ramezanpour, M.; Leung, S. S. W.; Delgado-Magnero, K. H.; Bashe, B. Y. M.; Thewalt, J.; Tieleman, D. P. Computational and experimental approaches for investigating nanoparticle-based drug delivery systems. *Biochim. Biophys. Acta, Biomembr.* **2016**, *1858*, 1688−1709.
(41) Bunker, A.; Róg, T. Mechanistic understanding from molecular dynamics simulation in pharmaceutical research 1: Drug delivery. *Front. Mol. Biosci.* **2020**, *7*, 604770.
(42) Wang, W.; Ye, Z.; Gao, H.; Ouyang, D. Computational pharmaceutics-A new paradigm of drug delivery. *J. Controlled Release* **2021**, *338*, 119−136.
(43) Bruininks, B. M.; Souza, P. C.; Ingolfsson, H.; Marrink, S. J. A molecular view on the escape of lipoplexed DNA from the endosome. *Elife* **2020**, *9*, No. e52012.
(44) Jayaraman, M.; Ansell, S. M.; Mui, B. L.; Tam, Y. K.; Chen, J.; Du, X.; Butler, D.; Eltepu, L.; Matsuda, S.; Narayanannair, J. K.; Rajeev, K. G.; Hafez, I. M.; Akinc, A.; Maier, M. A.; Tracy, M. A.; Cullis, P. R.; Madden, T. D.; Manoharan, M.; Hope, M. J. Maximizing the potency of siRNA lipid nanoparticles for hepatic gene silencing in vivo. *Angew. Chem.* **2012**, *124*, 8657−8661.
(45) Mercer, J. Investigating a model lipid nanoparticle release system with 2H NMR and SAXS. Doctoral Dissertation, Science: Department of Physics, 2018.
(46) Ramezanpour, M.; Schmidt, M. L.; Bashe, B. Y. M.; Pruim, J. R.; Link, M. L.; Cullis, P. R.; Harper, P. E.; Thewalt, J. L.; Tieleman, D. P. Structural properties of inverted hexagonal phase: A hybrid computational and experimental approach. *Langmuir* **2020**, *36*, 6668−6680.
(47) Rand, R. P.; Luzzati, V. X-ray diffraction study in water of lipids extracted from human erythrocytes: The position of cholesterol in the lipid lamellae. *Biophys. J.* **1968**, *8*, 125−137.
(48) Taylor, M. G.; Akiyama, T.; Smith, I. C. P. The molecular dynamics of cholesterol in bilayer membranes: A deuterium NMR study. *Chem. Phys. Lipids* **1981**, *29*, 327−339.
(49) Dufourc, E. J.; Parish, E. J.; Chitrakorn, S.; Smith, I. C. P. Structural and dynamical details of cholesterol-lipid interaction as revealed by deuterium NMR. *Biochemistry* **1984**, *23*, 6062−6071.
(50) Franks, N. P. Structural analysis of hydrated egg lecithin and cholesterol bilayers I. X-ray diffraction. *J. Mol. Biol.* **1976**, *100*, 345−358.
(51) Worcester, D. L.; Franks, N. P. Structural analysis of hydrated egg lecithin and cholesterol bilayers II. Neutron diffraction. *J. Mol. Biol.* **1976**, *100*, 359−378.
(52) Humphrey, W.; Dalke, A.; Schulten, K. VMD: Visual molecular dynamics. *J. Mol. Graphics Modell.* **1996**, *14*, 33−38.
(53) Berendsen, H. J. C.; van der Spoel, D.; van Drunen, R. GROMACS: A message-passing parallel molecular-dynamics implementation. *Comput. Phys. Commun.* **1995**, *91*, 43−56.
(54) Klauda, J. B.; Venable, R. M.; Freites, J. A.; O'Connor, J. W.; Tobias, D. J.; Mondragon-Ramirez, C.; Vorobyov, I.; MacKerell, A. D.; Pastor, R. W. Update of the CHARMM All-Atom Additive Force Field for Lipids: Validation on Six Lipid Types. *J. Phys. Chem. B* **2010**, *114*, 7830−7843.
(55) Ramezanpour, M.; Schmidt, M. L.; Bodnariuc, I.; Kulkarni, J. A.; Leung, S. S. W.; Cullis, P. R.; Thewalt, J. L.; Tieleman, D. P. Ionizable amino lipid interactions with POPC: Implications for lipid nanoparticle function. *Nanoscale* **2019**, *11*, 14141−14146.
(56) Durell, S. R.; Brooks, B. R.; Ben-Naim, A. Solvent-induced forces between 2 hydrophilic groups. *J. Phys. Chem.* **1994**, *98*, 2198−2202.
(57) Jorgensen, W. L.; Chandrasekhar, J.; Madura, J. D.; Impey, R. W.; Klein, M. L. Comparison of simple potential functions for simulating liquid water. *J. Chem. Phys.* **1983**, *79*, 926−935.
(58) Hess, B.; Bekker, H.; Berendsen, H. J. C.; Fraaije, J. G. E. M. LINCS: A linear constraint solver for molecular simulations. *J. Comput. Chem.* **1997**, *18*, 1463−1472.
(59) Grubmüller, H.; Heller, H.; Windemuth, A.; Schulten, K. Generalized Verlet algorithm for efficient molecular dynamics simulations with long-range interactions. *Mol. Simul.* **1991**, *6*, 121−142.
(60) Darden, T.; York, D.; Pedersen, L. Particle mesh Ewald: An N.log(N) method for Ewald sums in large systems. *J. Chem. Phys.* **1993**, *98*, 10089−10092.
(61) Essmann, U.; Perera, L.; Berkowitz, M. L.; Darden, T.; Lee, H.; Pedersen, L. G. A smooth particle mesh Ewald method. *J. Chem. Phys.* **1995**, *103*, 8577−8593.
(62) Nosé, S. A molecular-dynamics method for simulations in the canonical ensemble. *Mol. Phys.* **1984**, *52*, 255−268.
(63) Hoover, W. G. Canonical dynamics: Equilibrium phase-space distributions. *Phys. Rev. A* **1985**, *31*, 1695−1697.
(64) Parrinello, M.; Rahman, A. Polymorphic transitions in single-crystals: A new molecular-dynamics method. *J. Appl. Phys.* **1981**, *52*, 7182−7190.
(65) Nosé, S.; Klein, M. L. Constant pressure molecular-dynamics for molecular-systems. *Mol. Phys.* **1983**, *50*, 1055−1076.
(66) Berendsen, H. J. C.; Postma, J. P. M.; van Gunsteren, W. F.; Dinola, A.; Haak, J. R. Molecular dynamics with coupling to an external bath. *J. Chem. Phys.* **1984**, *81*, 3684−3690.
(67) Turner, D. C.; Gruner, S. M. X-ray diffraction reconstruction of the inverted hexagonal (HII) phase in lipid-water systems. *Biochemistry* **1992**, *31*, 1340−1355.
(68) Harper, P.; Mannock, D.; Lewis, R.; McElhaney, R.; Gruner, S. X-ray diffraction structures of some phosphatidylethanolamine lamellar and inverted hexagonal phases (2001, vol 81, pp: 2693). *Biophys. J.* **2012**, *102*, 1236.
(69) Chen, Z.; Rand, R. P. The influence of cholesterol on phospholipid membrane curvature and bending elasticity. *Biophys. J.* **1997**, *73*, 267−276.
(70) Giang, H.; Schick, M. On the puzzling distribution of cholesterol in the plasma membrane. *Chem. Phys. Lipids* **2016**, *199*, 35−38.
(71) Pan, J.; Tristram-Nagle, S.; Nagle, J. F. Effect of cholesterol on structural and mechanical properties of membranes depends on lipid chain saturation. *Phys. Rev. E* **2009**, *80*, 021931.
(72) Yesylevskyy, S. O.; Demchenko, A. P. Cholesterol behavior in asymmetric lipid bilayers: Insights from molecular dynamics simulations. *Methods in Membrane Lipids*; Humana Press: New York, NY, 2015; pp 291−306.
(73) Wassall, S.; Brzustowicz, M.; Shaikh, S.; Cherezov, V.; Caffrey, M.; Stillwell, W. Order from disorder, corralling cholesterol with chaotic lipids: The role of polyunsaturated lipids in membrane raft formation. *Chem. Phys. Lipids* **2004**, *132*, 79−88.

https://doi.org/10.1021/acs.langmuir.2c00430
Langmuir 2022, 38, 7462−7471

(74) Baumgart, T.; Hess, S. T.; Webb, W. W. Imaging coexisting fluid domains in biomembrane models coupling curvature and line tension. *Nature* **2003**, *425*, 821−824.
(75) Zhao, J.; Wu, J.; Heberle, F. A.; Mills, T. T.; Klawitter, P.; Huang, G.; Costanza, G.; Feigenson, G. W. Phase studies of model biomembranes: Complex behavior of DSPC/DOPC/cholesterol. *Biochim. Biophys. Acta, Biomembr.* **2007**, *1768*, 2764−2776.
(76) Ohvo-Rekilä, H.; Ramstedt, B.; Leppimäki, P.; Slotte, J. P. Cholesterol interactions with phospholipids in membranes. *Prog. Lipid Res.* **2002**, *41*, 66−97.
(77) Veatch, S. L.; Keller, S. L. Seeing spots: complex phase behavior in simple membranes. *Biochim. Biophys. Acta, Mol. Cell Res.* **2005**, *1746*, 172−185.
(78) Marsh, D. Cholesterol-induced fluid membrane domains: a compendium of lipid-raft ternary phase diagrams. *Biochim. Biophys. Acta, Biomembr.* **2009**, *1788*, 2114−2123.
(79) Baoukina, S.; Ingólfsson, H. I.; Marrink, S. J.; Tieleman, D. P. Curvature-Induced Sorting of Lipids in Plasma Membrane Tethers. *Adv. Theory Simul.* **2018**, *1*, 1800034.
(80) Kirk, G. L.; Gruner, S. M.; Stein, D. L. A thermodynamic model of the lamellar to inverse hexagonal phase transition of lipid membrane-water systems. *Biochemistry* **1984**, *23*, 1093−1102.
(81) Kirk, G. L.; Gruner, S. M. Lyotropic effects of alkanes and headgroup composition on the Lα-HII lipid liquid crystal phase transition: Hydrocarbon packing versus intrinsic curvature. *J. Phys.* **1985**, *46*, 761−769.
(82) Gruner, S. M. Intrinsic curvature hypothesis for biomembrane lipid composition: A role for nonbilayer lipids. *Proc. Natl. Acad. Sci. U.S.A.* **1985**, *82*, 3665−3669.
(83) Tate, M. W.; Gruner, S. M. Lipid polymorphism of mixtures of dioleoylphosphatidylethanolamine and saturated and monounsaturated phosphatidylcholines of various chain lengths. *Biochemistry* **1987**, *26*, 231−236.
(84) Cano-Sarabia, M.; Angelova, A.; Ventosa, N.; Lesieur, S.; Veciana, J. Cholesterol induced CTAB micelle-to-vesicle phase transitions. *J. Colloid Interface Sci.* **2010**, *350*, 10−15.
(85) Kuzmin, P. I.; Zimmerberg, J.; Chizmadzhev, Y. A.; Cohen, F. S. A quantitative model for membrane fusion based on low-energy intermediates. *Proc. Natl. Acad. Sci. U.S.A.* **2001**, *98*, 7235−7240.
(86) Martens, S.; Kozlov, M. M.; McMahon, H. T. How synaptotagmin promotes membrane fusion. *Science* **2007**, *316*, 1205−1208.
(87) Jahn, R.; Scheller, R. H. SNAREs—engines for membrane fusion. *Nat. Rev. Mol. Cell Biol.* **2006**, *7*, 631−643.
(88) Harrison, S. C. Viral membrane fusion. *Nat. Struct. Mol. Biol.* **2008**, *15*, 690−698.
(89) Chernomordik, L. V.; Kozlov, M. M. Mechanics of membrane fusion. *Nat. Struct. Mol. Biol.* **2008**, *15*, 675−683.
(90) Kulkarni, J. A.; Darjuan, M. M.; Mercer, J. E.; Chen, S.; Van Der Meel, R.; Thewalt, J. L.; Tam, Y. Y. C.; Cullis, P. R. On the formation and morphology of lipid nanoparticles containing ionizable cationic lipids and siRNA. *ACS Nano* **2018**, *12*, 4787−4795.
(91) Kobayashi, T.; Stang, E.; Fang, K. S.; de Moerloose, P.; Parton, R. G.; Gruenberg, J. A lipid associated with the antiphospholipid syndrome regulates endosome structure and function. *Nature* **1998**, *392*, 193−197.
(92) Van Meer, G.; Voelker, D. R.; Feigenson, G. W. Membrane lipids: where they are and how they behave. *Nat. Rev. Mol. Cell Biol.* **2008**, *9*, 112−124.
(93) Feller, S. E.; Pastor, R. W. On simulating lipid bilayers with an applied surface tension: Periodic boundary conditions and undulations. *Biophys. J.* **1996**, *71*, 1350−1355.
(94) Marrink, S. J.; Risselada, H. J.; Yefimov, S.; Tieleman, D. P.; De Vries, A. H. The MARTINI force field: coarse grained model for biomolecular simulations. *J. Phys. Chem. B* **2007**, *111*, 7812−7824.
(95) Souza, P. C. T.; Alessandri, R.; Barnoud, J.; Thallmair, S.; Faustino, I.; Grünewald, F.; Patmanidis, I.; Abdizadeh, H.; Bruininks, B. M. H.; Wassenaar, T. A.; Kroon, P. C.; Melcr, J.; Nieto, V.; Corradi, V.; Khan, H. M.; Domański, J.; Javanainen, M.; Martinez-Seara, H.; Reuter, N.; Best, R. B.; Vattulainen, I.; Monticelli, L.; Periole, X.; Tieleman, D. P.; de Vries, A. H.; Marrink, S. J. Martini 3: a general purpose force field for coarse-grained molecular dynamics. *Nat. Methods* **2021**, *18*, 382−388.
(96) Marrink, S. J.; De Vries, A. H.; Mark, A. E. Coarse grained model for semiquantitative lipid simulations. *J. Phys. Chem. B* **2004**, *108*, 750−760.

https://doi.org/10.1021/acs.langmuir.2c00430
Langmuir 2022, 38, 7462−7471